pubs.acs.org/Biomac

Article

Supramolecular Assembly and Small-Molecule Binding by Protein-Engineered Coiled-Coil Fibers

Dustin Britton, Julia Monkovic, Sihan Jia, Chengliang Liu, Farbod Mahmoudinobar, Michael Meleties, P. Douglas Renfrew, Richard Bonneau, and Jin Kim Montclare*

Cite This: https://doi.org/10.1021/acs.biomac.2c01031

Read Online

ACCESS | Metrics & More | Article Recommendations | Supporting Information

ABSTRACT: The ability to engineer a solvent-exposed surface of self-assembling coiled coils allows one to achieve a higher-order hierarchical assembly such as nano- or microfibers. Currently, these materials are being developed for a range of biomedical applications, including drug delivery systems; however, ways to mechanistically optimize the coiled-coil structure for drug binding are yet to be explored. Our laboratory has previously leveraged the functional properties of the naturally occurring cartilage oligomeric matrix protein coiled coil (C), not only for its favorable motif but also for the presence of a hydrophobic pore to allow for small-molecule binding. This includes the development of Q, a rationally designed pentameric coiled coil derived from C. Here, we present a small library of protein microfibers derived from the parent sequences of C and Q bearing various electrostatic potentials with the aim to investigate the influence of higher-order assembly and encapsulation of candidate small molecule, curcumin. The supramolecular fiber size appears to be well-controlled by sequence-imbued electrostatic surface potential, and protein stability upon curcumin binding is well correlated to relative structure loss, which can be predicted by *in silico* docking.

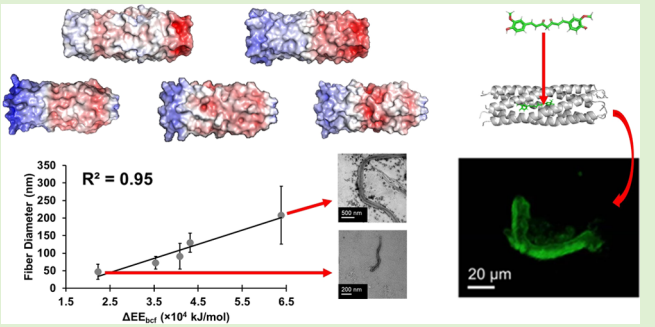

INTRODUCTION

Protein-engineered biomaterials have become an increasingly popular choice for a variety of biomedical and material-based applications including therapeutics and tissue-engineered scaffolds.[1−3] An important subset of these materials includes those that have the ability to self-assemble. In particular, self-assembling protein biomaterials possess ideal drug delivery potential, as they are both inherently biodegradable and can provide effective encapsulation of a variety of drugs and be easily modified for targeted drug release.[4,5] A protein biomaterial that has garnered increasing interest is the one that self-assembles into fibers. The formation of fibers is often the result of a variety of stimuli such as pH, temperature, concentration, ionic strength, and sequence; thus their formation can be readily tuned.[6]

Previous work has demonstrated that α-helical coiled-coil peptide domains can be designed to form nanofibers.[7−10] Particularly, the Woolfson group has studied the influence of electrostatics over thickness and stiffness in a designed protein fiber. They note the ability to promote thicker or thinner fibers by rationally charged mutations in smears or patches.[11,12] The control over self-assembly and fiber diameter, in particular, exists within the range of approximately 10−70 nm. Our group has also aimed to design and synthesize protein fibers of varying magnitudes of self-assembly from coiled-coil domains. We have previously utilized the self-assembling cartilage oligomeric matrix protein coiled coil (C) for generating biomaterials with the potential to encapsulate and deliver a wide variety of small-molecule therapeutics[13−15] and form nanofibers approximately 10−15 nm in diameter.[16] Included is the engineering of Q, based on the removal of the C-terminal heptad and swapping of the N- and C-terminus of C, which results in a positively and negatively charged patch at the N- and C-termini of its homopentameric coiled-coil domain.[15] Q displays the ability to form nanofibers up to 560 nm wide by the stacking of the oppositely charged ends of the domain, which is further capable of binding curcumin to form fibers 16 μm in diameter.[15]

We have defined a subset of three new coiled-coil protein variants for the study of protein nanofiber assemblies. We have defined a subset of three new coiled-coil protein variants, which we compare to C[13] and Q[14,15] for their ability to self-assemble. We elucidate the relationship between the protein electrostatic patches of the coiled coils while maintaining the ability to bind curcumin and undergo higher-order assembly

Received: August 21, 2022
Revised: September 29, 2022

into the mesoscale. We find that the electrostatic potential of surface-facing residues in the coiled coils has a direct correlation with the diameters of the supramolecular assembling fibers. Upon binding to curcumin, these protein fibers increase in diameter proportionally to their original fiber diameters without curcumin − becoming microns in diameters − and increase in thermostability proportionally to their relative loss of structure. Utilizing a combination of computational protein modeling and structural characterization, we further define the relationship between coiled-coil electrostatics and supramolecular assembly. As a result, we develop a novel, linear model for the prediction of the supramolecular assembly of our coiled-coil fibers. Importantly, we display the utility of using a uniquely and rationally derived electrostatic potential from Poisson−Boltzmann electrostatic calculations.

MATERIALS AND METHODS

Materials. Chemically competent M15MA *E. coli* cells were gifted from David Tirrell at the California Institute of Technology. Bactotryptone, sodium chloride (NaCl), yeast extract, tryptic soy agar (TSA), ampicillin sodium salt, sodium phosphate dibasic anhydrous (Na_2HPO_4), sodium hydroxide (NaOH), urea, dextrose monohydrate (D-glucose), magnesium sulfate ($MgSO_4$), calcium chloride ($CaCl_2$), manganese chloride tetrahydrate ($MnCl_2{\cdot}4H_2O$), cobaltous chloride hexahydrate ($CoCl_2{\cdot}6H_2O$), isopropyl β-D-1-thiogalactopyranoside (IPTG), Pierce bicinchoninic acid (BCA) assay kit, Pierce snakeskin dialysis tubing 3.5 K molecular weight cutoff (MWCO), sodium dodecyl sulfate (SDS), Nunc 96-well plates, and BD Clay Adams glass microscopy slides were acquired from Thermo Fisher Scientific. The 20 naturally occurring amino acids, dimethylsulfoxide (DMSO), nickel(III) chloride hexahydrate ($NiCl_2{\cdot}6H_2O$), sodium molybdate dihydrate ($Na_2MoO_4{\cdot}2H_2O$), iron(III) chloride ($FeCl_3$), iron(II) chloride tetrahydrate ($FeCl_2{\cdot}4H_2O$), thiamine hydrochloride (vitamin B), curcumin, and copper(II) sulfate pentahydrate ($CuSO_4{\cdot}5H_2O$) were purchased from Sigma Aldrich. Hydrochloric acid (HCl) and Coomassie Brilliant Blue G-250 were purchased from VWR. HiTrap FF 5 mL columns for protein purification were purchased from Cytiva Life Sciences. Macrosep and Microsep Advance Centrifugal Devices 3 K MWCO and 0.2 μm syringe filters were purchased from PALL. Acrylamide/bis solution (30%) 29:1 and natural polypeptide sodium dodecyl sulfate−polyacrylamide gel electrophoresis (SDS-PAGE) standard were purchased from Bio-Rad. Copper(II) chloride anhydrous ($CuCl_2$), sodium selenite (Na_2SeO_3), and imidazole were purchased from Acros Organics. Formvar/carbon-coated copper grids (FCF400-Cu) and 1% uranyl acetate for transmission electron microscopy were purchased from Electron Microscopy Sciences.

Computational Modeling and Docking of Protein and Curcumin. To assess the iterative effect of mutations on the stability of a coiled-coil protein variant and perform small-molecule docking simulations, the Rosetta suite of macromolecular modeling tools (Version 3.5) was used. Rosetta Relax protocol[17] was used on protein sequences using the symmetry of COMPcc (PDB: 3V2P) with the all-atom energy score function.[18] To dock curcumin (CCM) into the pore of a protein fiber variant, CCM conformer libraries were generated using the BioChemical Library BCL::Conformer Generation application.[19] Docking was performed in Rosetta using the GALigand Docking protocol in virtual high-screening mode (VSH)[20] to allow sampling of both the receptor and ligand conformational space. To accommodate the N- and C-terminal possible sites of the long and narrow cavity of the protein coiled coil,[21] CCM was docked with starting positions inside the first N-terminal half of the coiled coil and in the second C-terminal half of the coiled coil. One hundred models were generated from each starting conformation for a total of two hundred models, the best of which was used for analysis. Protein structures were visualized using PyMOL.[22] Spatial aggregation propensity (Sap) score was calculated in Rosetta with SapScore-Metric.[23]

Computational Calculation of Electrostatics. PDB2PQR software (version 3.1.0) was used to set up the titration states at room temperature with the amber[24] forcefield and propka[25] pH calculation method. Electrostatic maps and electrostatic potential energies were calculated using Adaptive Poisson−Boltzmann Solver (APBS) (Version 3.0.0) from subsequent PDB2PQR input files. In the calculation of the Rosetta score and electrostatic potential energy, the conserved His tag (sequence positions 1−17) is negated due to Rosetta's inability to define a consistent minimum energy state. The electrostatic potential energy difference between the termini was calculated using eq 1, where n is the sequence position number, l is the length of the sequence, and EE_{bcf} is the electrostatic potential energy of a residue if it is in the b, c, or f helical wheel position.

$$\Delta EE_{bcf} = \sum_{n=l/2}^{l} EE_{bcf} - \sum_{n=17}^{l/2-1} EE_{bcf} \quad (1)$$

Expression and Purification. C, C2, Q, Q2, and Q3 were all expressed and purified using the same protocol as follows. New variant plasmids (C2, Q2, and Q3) were cloned and purchased from Genscript in the PQE60 vector. Cloned plasmids were transformed into chemically competent methionine auxotrophic M15MA *E. coli* cells using heat shock. The transformed cells were grown for 16 h at 37 °C on TSA plates supplemented with 200 μg/mL ampicillin and 35 μg/mL kanamycin. Single colonies from the plate were used to inoculate 16 mL of supplemented M9 minimal media (0.5 M Na_2HPO_4, 0.22 M KH_2PO_4, 0.08 M NaCl, and 0.18 M NH_4Cl) containing all 20 natural amino acids (100 μg/mL), ampicillin (200 μg/mL), kanamycin (35 μg/mL), vitamin B (35 μg/mL), D-glucose (100 μg/mL), magnesium sulfate (1 mM), and calcium chloride (0.1 mM). Starter cultures were incubated at 37 °C and 350 rpm for 16 h. All 16 mL of starter culture was used to inoculate 400 mL of supplemented M9 minimal media, which was then incubated at 37 °C and 350 rpm. Expression of each protein was induced with the addition of 200 μg/mL IPTG once the optical density (OD_{600}) reached ∼0.8. Following 3 h of expression, cells were harvested by centrifuging for 30 min at 4000g at 4 °C in an Avanti J-25 centrifuge (Beckman Coulter) where resulting pellets were stored at −20 °C until purification.

All proteins were purified under denaturing conditions and pellets were resuspended in buffer A (50 mM NaH_2PO_4, 6 M urea, pH 8.0). Lysis was performed using a Q500 sonicator at 50% amplitude and 5 s on and 5 s off pulse sequence for a total time of 2.5 min. Cell lysates were then centrifuged at 14,000g for 50 min at 4 °C to remove cell debris. The supernatant was purified using a syringe-pump driven IMAC Sepharose high-performance 5 mL column (HiTrap Q HP 5, Cytvia) charge with $CoCl_2$. The protein was eluted using an increasing concentration of buffer B (50 mM NaH_2PO_4, 6 M urea, 500 mM imidazole, pH 8.0) with buffer A ranging from 0 to 100% v/v. Elutions were collected and run on a 12% SDS-PAGE. Pure elutions were removed and dialyzed using 3.5 kDa MWCO tubing at 4 °C in 5 L volumes using stepwise concentrations of 3, 1.5, and 0.75 M urea in 50 mM NaH_2PO_4 at pH 4.0, followed by six 5 L volumes of buffer composed of 50 mM NaH_2PO_4 at pH 4.0. Protein was then concentrated to approximately 1.5 mL using 3 kDa MWCO Macrosep and Microsep Advance centrifugal devices (Pall Corporation) at 3000g. Protein concentration was then determined by a bicinchoninic acid (BCA) assay with a standard curve based on bovine serum albumin concentrations.

Circular Dichroism Spectroscopy. The secondary structure was first assessed using a Jasco J-815 CD spectrometer with a PTC-423S single-position Peltier temperature control system. Wavelength scans were performed from 190 to 250 nm using 15 μM samples at 1 nm step sizes at 25 °C. Temperature scans were performed at the α-helical minimum of 222 nm from 20 to 85 °C. The mean residue ellipticity (MRE) was calculated as described previously.[13] MREs at 222 and 208 nm and their ratios were used to assess relative helicity.

Attenuated Total Reflectance-Fourier Transform Infrared Spectroscopy. The secondary structure of protein fiber variants was confirmed using attenuated total reflectance-Fourier transform

https://doi.org/10.1021/acs.biomac.2c01031
Biomacromolecules XXXX, XXX, XXX−XXX

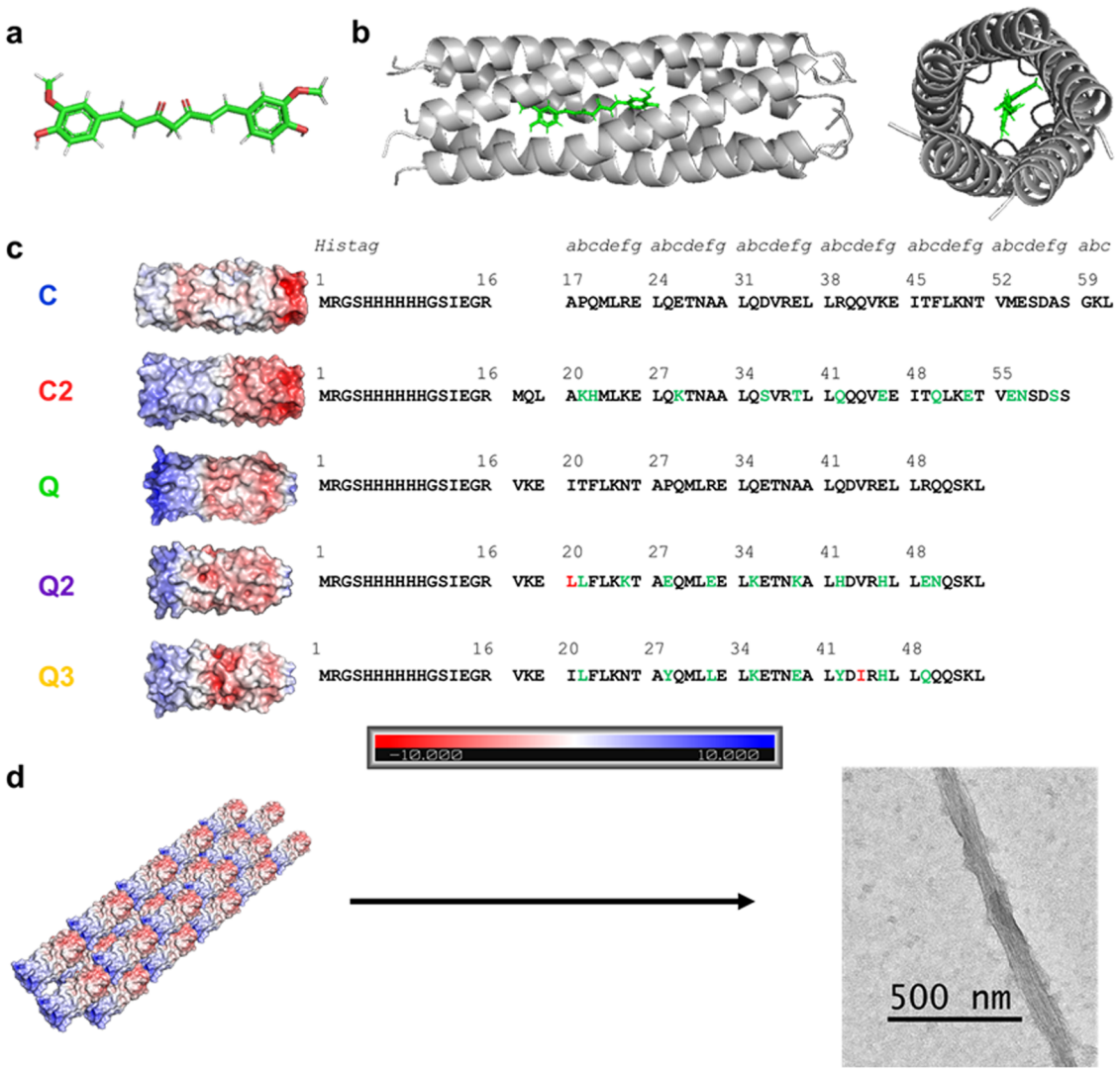

Figure 1. (a) Curcumin molecular structure. (b) C as an example of a coiled coil with curcumin docked in the favorable N-terminal position. (c) Coiled-coil library based on C and Q with sequence information and electrostatic potential maps with positive blue patches and negative red patches with scale −10 to 10 kbT. Mutations to the solvent-exposed residues in the *b*, *c*, and *f* helical wheel positions are in green and mutations of the hydrophobic pore in *a* and *d* helical wheel positions are in red. (d) Schematic of coiled-coil stacking end-to-end to comprise a nanoscale fiber (example TEM image).

infrared (ATR-FTIR) spectroscopy using a Nicolet 6700 Fourier transform infrared spectrometer equipped with a diamond ATR accessory and a mercury cadmium telluride (MCT)-A detector. Spectra were collected for 5 μL of 500 μM protein from 4000 to 400 cm^{-1} with 0.5 cm^{-1} increments at room temperature (RT). For CCM-bound protein, the protein was bound at a final concentration of 500 μM and saturated with CCM as determined by fluorescent spectroscopic drug binding with a final 1% v/v DMSO. The sample spectra were normalized using a buffer background and analyzed from 1700 to 1600 cm^{-1}, corresponding to the amide I region. Peaks were deconvoluted using Gaussian functions in PeakFit software until the goodness of fit reached $r^2 \geq 0.99$.[26,27] Peaks associated with the secondary structure were determined as described by Jackson et al.[28]

Transmission Electron Microscopy. Transmission electron microscopy (TEM) images were taken with an FEI Talos L120C transmission electron microscope. Protein fiber samples were diluted to 50 μM and 3 μL and were spotted on Formvar/carbon-coated copper grids followed by 5 μL wash with water, and 3 μL staining with 1% v/v uranyl acetate solution each with incubation times of 1 min at RT. Fibrils were sized in ImageJ software (Version 1.52q).[29]

Drug Binding. Protein variants were bound to curcumin (CCM) in the increasing CCM:protein ratios from 1:1 to 10:1. The protein was diluted to a final concentration of 15 μM before CCM solubilized in DMSO was added to the protein sample at a final 1% v/v DMSO. The samples were incubated on a thermomixer for 30 min at 300 rpm in the dark at 4 °C. The samples were then removed and 300 μL of each sample was added to a 96-well solid black plate. Protein variants were excited at 420 nm and emission was read at 520 nm using a BioTek Synergy H1 microplate reader at RT. The baseline spectra of CCM, at 15−150 μM in 50 mM PB pH 4.0 containing 1% v/v DMSO, were subtracted from the fluorescence intensities of the protein−CCM at corresponding concentrations. The resulting normalized relative fluorescence intensities were analyzed using specific binding kinetics in GraphPad Prism (GraphPad Software).

Confocal Microscopy. The protein bound to CCM was studied by measuring 50 μM protein samples saturated with CCM as determined by fluorescent spectroscopic drug binding with a final 1% v/v DMSO (or 2 × K_d). Ten microliters of protein was added to a microslide and a 22 × 22 mm #1 microscope cover glass. The slides were inverted and imaged using a Leica TCS SP8 X laser confocal microscope using a dry 10× objective at RT. CCM was excited using a 460 nm line of the laser, and images were taken using a 470−550 nm detection window.

https://doi.org/10.1021/acs.biomac.2c01031
Biomacromolecules XXXX, XXX, XXX−XXX

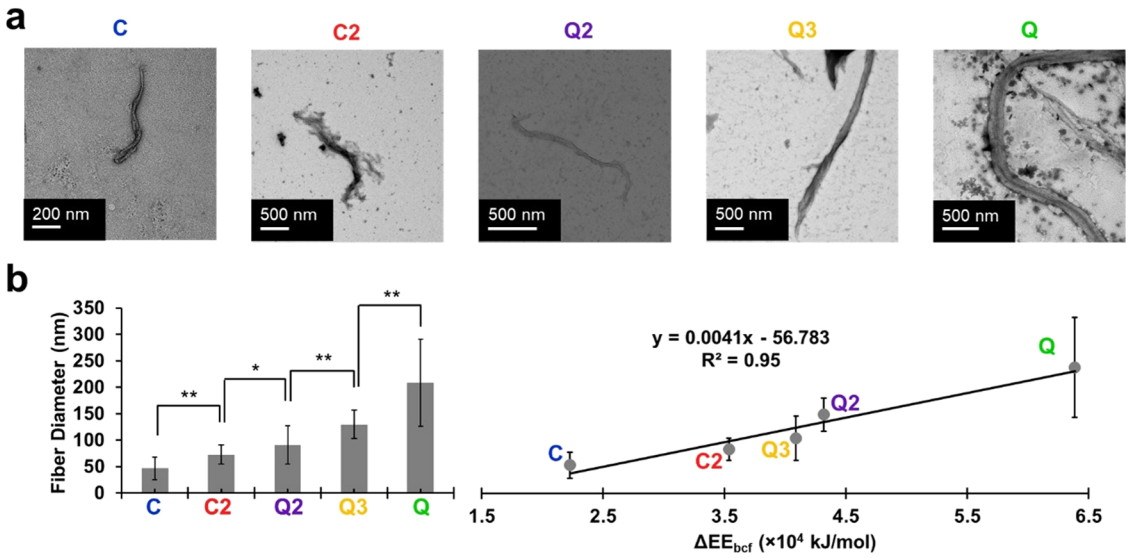

Figure 2. (a) Representative TEM images of protein fiber variants in the order of ascending size. (b) Average fiber diameters of protein fiber variants (* indicates p-value < 0.05 and ** indicates p-value < 0.01 by unpaired t-test) and as plotted against the cumulative electrostatic potential energy difference of each terminus of solvent-exposed residues in the b, c, and f helical wheel positions (ΔEE_{bcf}). Average and standard deviation are the result of 20 fiber measurements using ImageJ.

Statistical Analysis. GraphPad Prism (GraphPad Software) was employed for statistical analysis using Student's t-test.

RESULTS AND DISCUSSION

Coiled-Coil Minilibrary Design. A minilibrary was designed with a breadth of electrostatic distributions while retaining a positively and negatively charged patch on the N- and C-termini, respectively. Previously studied protein sequences C and Q were also used in the library (Figure 1).

First Q2 was designed to undergo reduced lateral assembly. The protonation and deprotonation of solvent-exposed residues are believed to be the key factor affecting the self-assembly of Q into fibers. Using Rosetta, the charge in the solvent-exposed b, c, and f positions was modified to (1) redistribute the surface to be more negative and lower the pI; (2) lower the overall electrostatic potential energy (U_E); and (3) improve the Rosetta stability score. A more evenly distributed negative surface on the C-terminus was hypothesized to push the pI to be more neutral and balance the positive and negative surface patches resulting from the largely positive patch constituted by the N-terminus and His tag. Recent studies, including that by our group, on electrostatically interacting coiled coils have shown a strong correlation between the gelation kinetics and overall charge of the protein where faster gelation and an increased storage modulus are seen at pH near the pI of the protein.[30,31] A lower overall U_E is hypothesized to preferentially decrease the lateral interaction of the neighboring coiled coils since end-to-end protofibril stacking is conserved from C-derived coiled-coil fibers.[13−15] Mutations are rationally chosen and iteratively checked using the Rosetta relax score functions and APBS electrostatic potential energy (U_E) until these goals are achieved. Complementary to the redistribution of the surface charge, hydrophobic residues necessary for helix and coiled-coil formation are maintained throughout the surface charge optimization. A single-point mutation, I20 L, is then made in the hydrophobic pore to further stabilize it from changes in temperature for future studies. A final design of Q2 exhibits a more neutral pI of 8.2 compared to 9.7 for Q.

Two additional sequences have been conceived to elucidate the relationship to electrostatic, self-assembly, and CCM binding studied here: one based on the Q domain and another based on the C domain (to establish that redistribution and self-assembly might be controlled for pentamers not based solely on the Q domain). Similar criteria to the design of Q2 have been used to generate sequences with electrostatic diversity on the surface where mutations are constricted to the solvent-exposed b, c, and f helical wheel positions using Rosetta. C2 is generated by redistribution of the electrostatic patches of C such that a more negatively charged patch is represented on the surface of the C-terminus in the electrostatic map and a more positively charged patch is represented on the surface of the N-terminus in the electrostatic map. Similarly, Q3 is designed to redistribute the electrostatic potential into a unique electrostatic potential map, and this time with a preferred hydrophobic pore mutation V44I as determined by Rosetta. Both variants have been designed by iterative mutations that were rationally chosen and checked for equal or improved stability using the Rosetta relax, score functions, and APBS electrostatic potential maps. The resulting Rosetta scores are −760 kcal/mol for C, −777 kcal/mol for C2, −619 kcal/mol for Q, −637 kcal/mol for Q2, and −624 kcal/mol for Q3.

Electrostatics and Fiber Assembly. Protein variants were successfully purified (Figures S1−S5) and concentrated to approximately 1 mM in 50 mM NaH_2PO_4 buffer at pH 4.0. Proteins were first confirmed to maintain their ability to undergo supramolecular assembly by TEM (Figures 2a and S6). All variants studied demonstrated the formation of nanoscale fibers. Average protein fiber diameters were ranked from smallest to largest with 47 ± 22 nm for C, 73 ± 18 nm for C2, 91 ± 37 nm for Q2, 130 ± 27 nm for Q3, and 208 ± 82 nm for Q (Figure 2b). By conventional criteria (p-value < 0.05), protein fiber diameters were all calculated by an unpaired t-test to be significantly different from each other.

Since the large fiber assemblies seen previously in Q[15,31,32] are the result of electrostatic coupling and the end-to-end alignment of coiled coils, we hypothesize that the quantifica-

https://doi.org/10.1021/acs.biomac.2c01031
Biomacromolecules XXXX, XXX, XXX−XXX

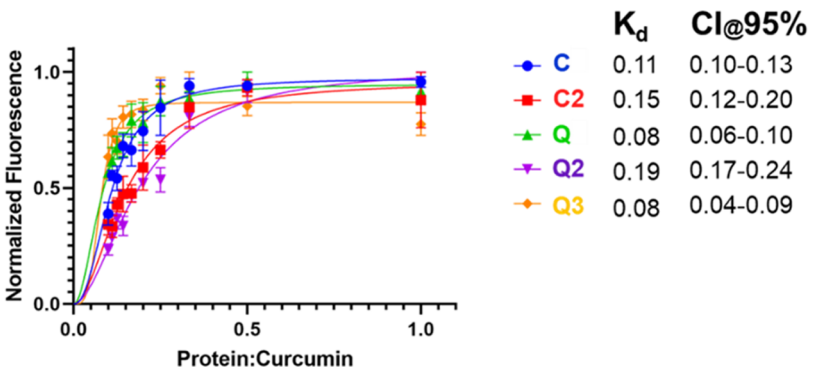

Figure 3. Spectroscopic fluorescence of protein fiber variants at different protein:curcumin ratios. Fluorescence was measured by excitation at 420 nm and emission at 520 nm. Error bars and confidence interval (CI@95%) represent the standard deviation of three independent results.

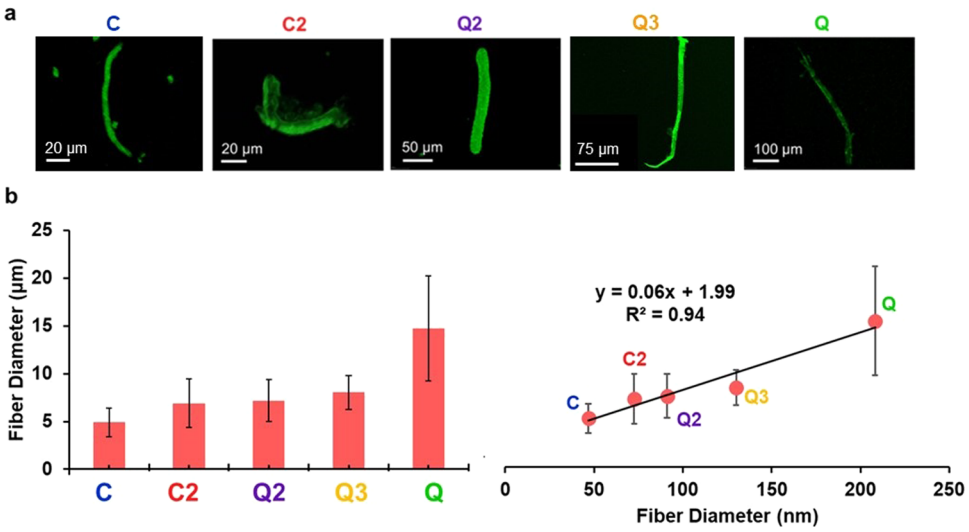

Figure 4. (a) Fluorescent confocal microscopy images of protein fiber variants after CCM binding using 460 nm excitation and a 470−550 nm detection window. (b) Average diameter of protein fiber variants after CCM binding as measured by confocal microscopy and correlated to average protein fiber diameter variants measured by TEM. Average and standard deviation are the result of 20 fiber measurements using ImageJ.

tion of the electrostatic patches that comprise these fibers might be correlated to the ability to undergo supramolecular fiber assembly. Using the Poisson−Boltzmann electrostatic potential calculated from APBS, we assessed the cumulative electrostatic potential energy difference of each terminus (split halfway in the sequence) calculated from the solvent-exposed residues in the b, c, and f positions (ΔEE_{bcf}) as seen in eq 1. The growth in diameter appears to also increase in a nearly exponential manner. This difference is strongly correlated to a linear relationship (R^2 = 0.95) with the average observed fiber diameters by TEM (Figure 2b).

To confirm that the change in fiber diameter is not the result of a change in surface hydrophobicity, the spatial aggregation propensity (Sap) score[23] was used to calculate the relative aggregation between protein fiber variants of residues in the b, c, and f helical wheel positions. While the scores presented a slight negative correlation with fiber diameter (R^2 = 0.60), it was significantly weaker than that from the ΔEE_{bcf} calculation noted above (Figure S7), and the correlation is strongly influenced by the much lower Sap score exhibited by Q. Additionally, a higher Sap score is expected to correlate to increased aggregation contrary to the correlation. It is important to note that while increased fiber growth is thought to occur by electrostatic coupling, the reduction of hydrophobic coupling may also assist or allow for increased fiber growth. Overall, our findings strengthen the conclusion that the supramolecular assemblies of our coiled-coil proteins are driven by the electrostatic potential of positively and negatively charged patches in the fiber. Moreover, this shows that the morphology of the protein assemblies may be tuned by selective mutations to the solvent-exposed surface of a coiled coil.

Curcumin Binding and Fiber Thickening. Previously, C and Q have exhibited a promiscuous binding site capable of binding small hydrophobic molecules.[13−16] We bound the small-molecule curcumin (CCM) to Q as a candidate molecule for drug delivery previously,[15] since the compound has been used therapeutically due to its antiproliferative, antibacterial, and anti-inflammatory properties.[33−35] We explicitly confirm the conservation of this binding pocket in these protein fiber variants by fluorescence spectroscopy (Figure 3) where the binding behavior is similar across all variants. Specific binding kinetics have been used to calculate the K_d of the fluorescence curves. Using 2 × K_d to calculate the saturation of CCM binding, we infer that one CCM molecule binds approximately three to six protein monomers on average.

Curcumin has also previously been known to induce fiber thickening of protein fibers including collagen[36,37] and Q[15] using CD, surface tension, and viscosity. The fiber thickening by CCM is driven by the interaction of negatively charged

https://doi.org/10.1021/acs.biomac.2c01031
Biomacromolecules XXXX, XXX, XXX−XXX

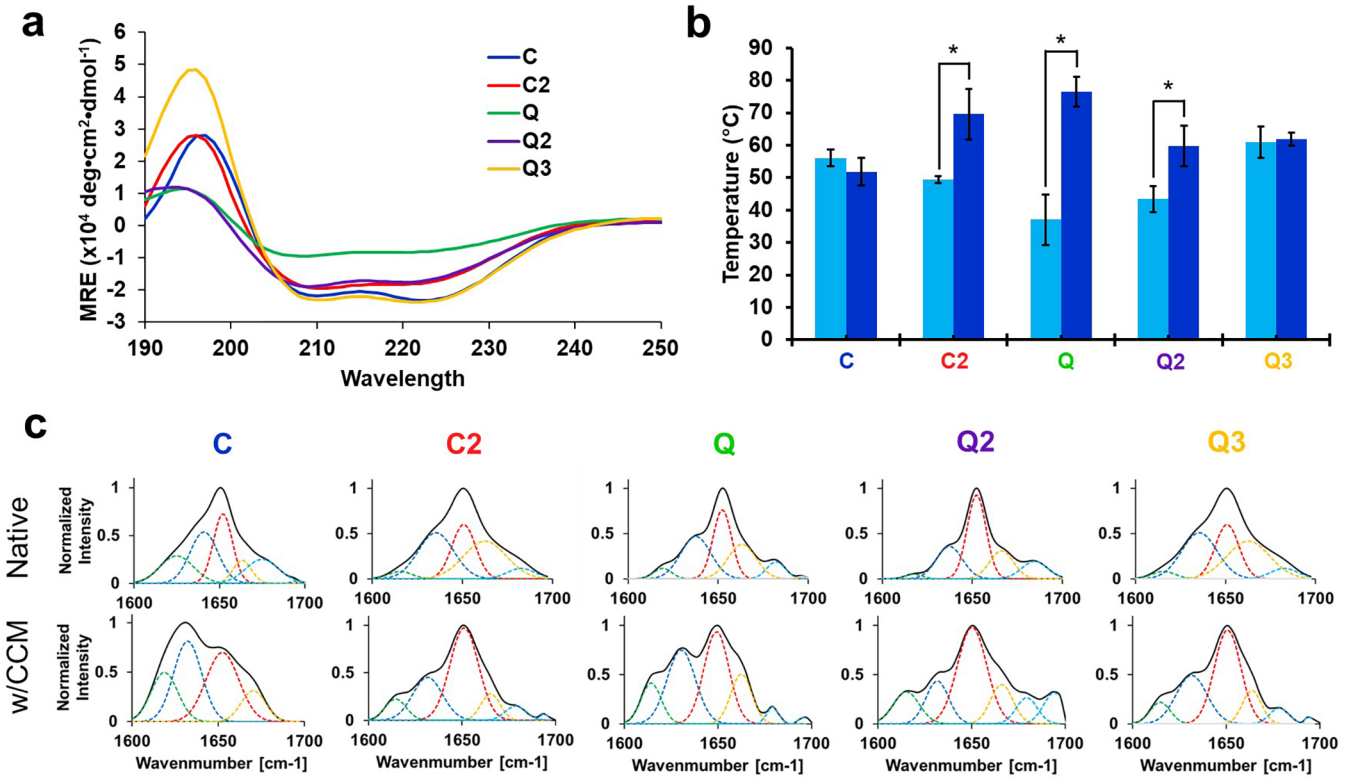

Figure 5. (a) Circular dichroism spectra of protein fiber variants at 25 °C. (b) Melting temperatures of native (light blue) and CCM-bound (dark blue) protein fiber variants as measured by CD (* indicates p-value < 0.05 by unpaired t-test). (c) Representative ATR-FTIR spectra of native and CCM-bound protein fiber variants. The black line represents fit to raw data. The red line represents a deconvoluted α-helical peak. The dark blue line represents the antiparallel β-sheet peak. The light blue line represents β-sheet peaks. The green line represents aggregated strand peaks. The yellow line represents 3−10 helix peaks. Error bars represent the standard deviation as a result of three independent trials.

residues on the surface of the protein with CCM while it is fully protonated in a low-pH system. Fathima et al. noted that this interaction assists in solvating polar groups on the surface and burying hydrophobic residues.[37] Furthermore, Fathima et al. note that CCM causes a local restructuring of water molecules, leading to increased protein surface activity and exposure of nonpolar groups,[36] which creates the driving force for protein−protein interaction or induced thickening of α-helical protein fibers in an effort to reduce surface energy. In our studies of Q using increased concentrations of CCM, CD measurements show that helical packing is unaffected and confirm that protein conformation is maintained.[15]

Using confocal microscopy, we test the relative thickening upon CCM binding in our coiled-coil variants (Figures 4a and S8). In the case of Q, the addition of CCM increased the diameter of the fiber to 14.74 ± 5.501 μm, consistent with our prior studies.[15] The protein variants further assemble into mesoscale fibers with diameters of 8.04 ± 1.78 μm for Q3, 7.17 ± 2.19 μm for Q2, 6.89 ± 2.54 μm for C2, and 4.91 ± 1.49 μm for C (Figure 4b). Notably, the fibers appear to proportionally thicken compared to their original fiber assemblies shown in Figure 2. We confirm this correlation by comparing the fiber diameters (by TEM) to the protein−CCM fiber diameters (by confocal microscopy) (Figure 4b) with a directly proportional relationship possessing an R^2 = 0.94; fiber thickening is not only present in all our protein variants but is also dependent on the original self-assembly properties (and thus electrostatics) of the fibers, independent of CCM.

Structure and Thermostability. To assess the secondary structure of the proteins, CD and ATR-FTIR measurements were performed (Figure 5). The CD wavelength scans could not be performed on protein after CCM binding since binding experiments used DMSO to solubilize CCM, which interfered with the measurement through strong absorbance of far-UV light.[38] CD spectra of all protein variants exhibited a double minimum at 222 and 208 nm, indicative of the α-helical content (Figure 5a and Table S1). Q displayed the lowest amount of helical content with minima −8000 ± 3000 and −10,000 ± 6000 deg·cm^2·dmol^{-1} at 222 and 208 nm, respectively. Previous studies of Q agreed with a dampened signal in CD measurements, which was proposed to be due to re-ordering of the heptads such that residue P28 resided at the center of Q.[15] Variants Q2 and Q3 possessing mutations P28E and P28Y, respectively, and possessing similar helical signal intensity to C and C2 confirmed the negative impact of the P28 mutation on Q α-helicity. The remaining coiled-coil proteins displayed an average double minima of −21,000 ± 5000 deg·cm^2·dmol^{-1} at 208 nm and −20,000 ± 6000 deg·cm^2·dmol^{-1} at 222 nm. Similarly, all proteins exhibited strong coiled-coil content in the range of 0.91−1.11 (Table S1), where helical systems with a 222/208 ratio > 1 indicated that the α-helix was found within a coiled-coil structure rather than in isolation.[39−41]

ATR-FTIR measurements were used to assess the secondary structure and compare proteins before and after binding to CCM (Tables S2−S6). Prior to CCM binding (native), protein variants showed a high order of structured content with a strong presence of α-helicity, in agreement with CD measurements. Q exhibited the weakest helical composition with a value of 32.8 ± 4.2% and the highest percentage of

https://doi.org/10.1021/acs.biomac.2c01031
Biomacromolecules XXXX, XXX, XXX−XXX

random content with a value of 25.1 ± 10.3% (Tables S2−S6). In contrast, Q2 demonstrated the strongest helical percent composition of 50.8 ± 6.0%, and C2 demonstrated the weakest random percent composition of 9.4 ± 7.2% (Tables S2−S6). In comparison, after binding to CCM, all of the proteins experienced a consistent loss in the structured content, noted by the broadening of the amide II bond region curves comprised of random coil content signals in the ranges of 1610−1628 and 1660−1670 cm^{-1}, respectively (Figure 5c).[28]

The melting temperatures of the proteins as measured by CD also experienced a shift as a result of curcumin binding. The melting temperatures for C and Q were 56.0 ± 2.6 and 37.0 ± 7.8 °C, respectively, at pH 4.0. Previously, C resulted in a melting temperature of 41−42 °C in Na_2HPO_4 at pH 8.0.[13,14] Q showed melting temperatures of 55.3, 63.5, and 46.4 °C in 50 mM Na_2HPO_4 at pH 4.0, 8.0, and 10.0, respectively,[15] and 39 °C in 50 mM Na_2HPO_4 at pH 8.0[14] in previous studies. Notably, the melting temperature of Q was sensitive to changes in buffer composition and pH. Here, in comparison, proteins were measured in 50 mM NaH_2PO_4 at pH 4.0, which would provide a lower ionic strength buffer than that used in previous studies. The melting temperatures of the protein variants were measured as 49.4 ± 1.1 °C for C2, 43.4 ± 4.0 °C for Q2, and 61.0 ± 4.9 °C for Q3 (Figure 5b). After binding to CCM, C2, Q1, and Q2 all experienced a significant change in melting temperature compared to their unbound states with p-values of 0.012, <0.001, and 0.019 by an unpaired t-test, respectively. All CCM-bound proteins resulted in melting temperatures greater than 50 °C, i.e., 51.8 ± 4.3 °C for C, 69.6 ± 7.8 °C for C2, 76.4 ± 4.6 °C for Q, 59.9 ± 6.3 °C for Q2, and 61.9 ± 2.0 °C for Q3 (Figure 5b).

To help decipher the impact of CCM binding on the protein, the Rosetta macromolecular suite was used to dock CCM and score the protein before and after docking. The best-scoring complexes were used to extract the Rosetta score of the protein (with and without the CCM ligand). Protein variants exhibited interface scores of −45.4 kcal/mol for C, −20.6 kcal/mol for C2, −46.2 kcal/mol for Q, −46.3 kcal/mol for Q2, and −45.2 kcal/mol for Q3, affirming the promiscuity of the C and Q binding pockets.[4,13−15] The lesser interface score exhibited by C2 as compared to its parent, C, can be explained by the absence of hydrogen bonding with the glutamic acid ring at the sequence position 54 (Figure S9) due to the decrease in the distance (0.3 Å) between chains at the C-terminus measured by PyMOL of the lowest-scoring poses preventing C-terminal encapsulation. When comparing the percent change of the protein Rosetta score before and after docking, a strong correlation (R^2 = 0.93) was found with the percent difference of the change in melting temperature (ΔT_m%) (Figure 6). The binding of curcumin positively impacted the stability of the fiber pentamer.

At the same time, a loss of structure is observed by ATR-FTIR measurements (Figure 7a). To elucidate this interplay of structure and stability, we define a relationship between the change in stability and the change in structure. We note that upon CCM binding, a greater increase in stability linearly correlates to a smaller loss in structured content (denoted by secondary structure not associated with a random coil content in ATR-FTIR) with an R^2 = 0.96 (Figure 7 and Tables S2−S6). Thus, while CCM binding imposes a negative impact on the ordered structure of the protein fibers based on the ATR-FTIR, CCM imparts a positive interaction in the pore of the coiled coil. Based on the y-intercept of the linear relationship

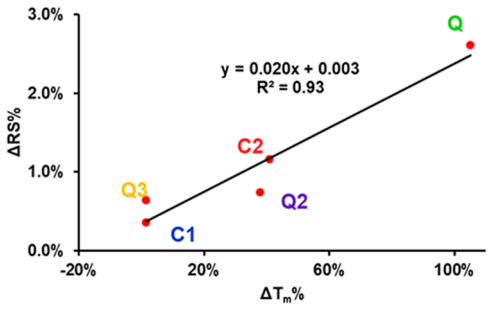

Figure 6. Correlation between the percent difference in the melting temperature (ΔT_m%) after binding CCM as measured by circular dichroism to percent difference in the protein Rosetta score (ΔRS%) after docking CCM.

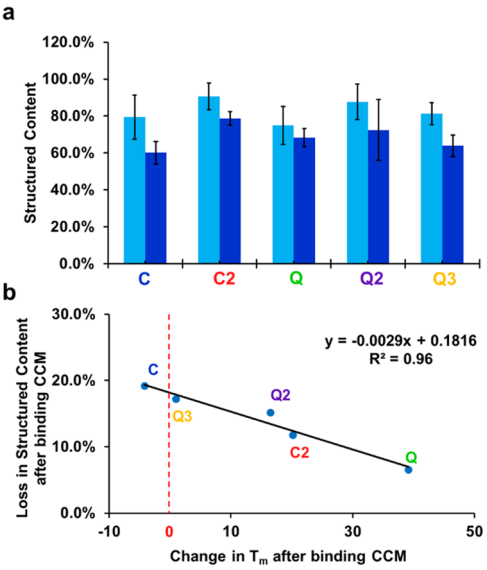

Figure 7. (a) Structured content of protein fiber variants before CCM binding (light blue) and after CCM binding (dark blue) as measured by peak deconvolution of three independent ATR-FTIR measurements. (b) Correlated structured content loss with change in T_m after binding to CCM. Error bars represent the standard deviation of three independent trials.

denoted in Figure 7b, this interaction appears to stabilize the pentameric interface and increases thermostability when the loss of structure is less than 18.2%. When the loss of structure is greater than 18.2% as in the case of C, the difference in T_m of the native and CCM-bound protein fibers (Figure 7b) indicates a continuation of this trend, where a greater loss in structure begins to cause a decrease in the thermostability of the protein.

CONCLUSIONS

We have designed and synthesized a minilibrary of coiled-coil proteins with mutations to create a diverse set of electrostatic distributions on the surface of the coiled-coil surface. We have assessed the ability of these coiled coils to undergo supramolecular assembly into nanoscale fibers of different degrees and correlated this relationship to the magnitude of the electrostatic potential difference of the surface. Furthermore, all fiber variants can bind the candidate small hydrophobic molecule, curcumin, which induces fiber assembly into the mesoscale. The relationship between the electrostatic potential of the surface and the resulting diameters after

https://doi.org/10.1021/acs.biomac.2c01031
Biomacromolecules XXXX, XXX, XXX−XXX

curcumin binding is maintained. While curcumin binding consistently induces a loss of structure, the binding of the small molecule appears to have a positive interaction in the hydrophobic pore that competes to improve thermostability.

As a result of these studies, we have developed a novel model for the prediction of the supramolecular assembly of coiled-coil proteins using a diverse set of sequences. Notably, the model is based on a novel and rationally designed metric, ΔEE_{bcf}, allowing for a simple calculation for the prediction of coiled-coil protein self-assembly. In addition to our thermostability studies, our discoveries show that coiled-coil proteins can be potentially predicted for supramolecular assembly and structure loss upon small-molecule binding completely *in silico*. Importantly, this discovery provides a strong foundation for material development and quantitative modeling of other protein systems using supramolecular assembling proteins and protein−protein interactions founded primarily on electrostatics.

■ ASSOCIATED CONTENT

Supporting Information

The Supporting Information is available free of charge at https://pubs.acs.org/doi/10.1021/acs.biomac.2c01031.

Supporting figures and tables including figures for protein purification, Sap scores vs. protein fiber diameter, additional transmission electron micrographs of fibers at various resolutions, additional confocal fluorescence microscopy images, best-scoring poses in PyMOL, tables for composition quantification of FTIR deconvolutions, and minima quantification for helical fiber spectra (PDF)

■ AUTHOR INFORMATION

Corresponding Author

Jin Kim Montclare − *Department of Chemical and Biomolecular Engineering, New York University Tandon School of Engineering, Brooklyn, New York 11201, United States; Bernard and Irene Schwartz Center for Biomedical Imaging, Department of Radiology, New York University School of Medicine, New York, New York 10016, United States; Department of Chemistry, New York University, New York, New York 10012, United States; Department of Biomaterials, New York University College of Dentistry, New York, New York 10010, United States;* orcid.org/0000-0001-6857-3591; Email: montclare@nyu.edu

Authors

Dustin Britton − *Department of Chemical and Biomolecular Engineering, New York University Tandon School of Engineering, Brooklyn, New York 11201, United States*

Julia Monkovic − *Department of Chemical and Biomolecular Engineering, New York University Tandon School of Engineering, Brooklyn, New York 11201, United States*

Sihan Jia − *Department of Chemical and Biomolecular Engineering, New York University Tandon School of Engineering, Brooklyn, New York 11201, United States*

Chengliang Liu − *Department of Chemical and Biomolecular Engineering, New York University Tandon School of Engineering, Brooklyn, New York 11201, United States*

Farbod Mahmoudinobar − *Department of Chemical and Biomolecular Engineering, New York University Tandon School of Engineering, Brooklyn, New York 11201, United States; Center for Computational Biology, Flatiron Institute, New York, New York 10010, United States*

Michael Meleties − *Department of Chemical and Biomolecular Engineering, New York University Tandon School of Engineering, Brooklyn, New York 11201, United States*

P. Douglas Renfrew − *Center for Computational Biology, Flatiron Institute, New York, New York 10010, United States*

Richard Bonneau − *Center for Computational Biology, Flatiron Institute, New York, New York 10010, United States*

Complete contact information is available at: https://pubs.acs.org/10.1021/acs.biomac.2c01031

Author Contributions

The manuscript was written through contributions of all authors. All authors have given approval to the final version of the manuscript.

Funding

This work was supported by NSF-DMREF under Award Number DMR 1728858 and the NSF-MRSEC Program under Award Number DMR 1420073. ATR-FTIR and confocal microscopy experiments were performed at the NYU Chemistry Department Shared Instrument Facility.

Notes

The authors declare no competing financial interest.

■ REFERENCES

(1) Sengupta, D.; Heilshorn, S. C. Protein-engineered biomaterials: highly tunable tissue engineering scaffolds. *Tissue Eng., Part B* **2010**, *16*, 285−293.

(2) Katyal, P.; Mahmoudinobar, F.; Montclare, J. K. Recent trends in peptide and protein-based hydrogels. *Curr. Opin. Struct. Biol.* **2020**, *63*, 97−105.

(3) Katyal, P.; Meleties, M.; Montclare, J. K. Self-Assembled Protein- and Peptide-Based Nanomaterials. *ACS Biomater. Sci. Eng.* **2019**, *5*, 4132−4147.

(4) Yin, L.; Agustinus, A. S.; Yuvienco, C.; Miniashima, T.; Schnabel, N. S.; Kirsch, T.; Montclare, J. K. Engineered Coiled-Coil Protein for Delivery of Inverse Agonist for Osteoarthritis. *Biomacromolecules* **2018**, *19*, 1614−1624.

(5) Maham, A.; Tang, Z.; Wu, H.; Wang, J.; Lin, Y. Protein-based nanomedicine platforms for drug delivery. *Small* **2009**, *5*, 1706−1721.

(6) Sun, S.; Su, Z.; Wei, G.2 - Self-assembly Formation of Peptide and Protein Nanofibers on Surfaces and At Interfaces. In *Artificial Protein and Peptide Nanofibers*, Wei, G.; Kumbar, S. G., Eds.; Woodhead Publishing, 2020; pp 23−39.

(7) Kojima, S.; Kuriki, Y.; Yoshida, T.; Yazaki, K.; Miura, K.-i. Fibril Formation by an Amphipathic α-Helix-Forming Polypeptide Produced by Gene Engineering. *Proc. Jpn. Acad., Ser. B* **1997**, *73*, 7−11.

(8) Bromley, E. H.; Channon, K. J.; King, P. J.; Mahmoud, Z. N.; Banwell, E. F.; Butler, M. F.; Crump, M. P.; Dafforn, T. R.; Hicks, M. R.; Hirst, J. D.; Rodger, A.; Woolfson, D. N. Assembly pathway of a designed alpha-helical protein fiber. *Biophys. J.* **2010**, *98*, 1668−1676.

(9) Papapostolou, D.; Bromley, E. H.; Bano, C.; Woolfson, D. N. Electrostatic control of thickness and stiffness in a designed protein fiber. *J. Am. Chem. Soc.* **2008**, *130*, 5124−5130.

(10) Ogihara, N. L.; Ghirlanda, G.; Bryson, J. W.; Gingery, M.; DeGrado, W. F.; Eisenberg, D. Design of three-dimensional domain-swapped dimers and fibrous oligomers. *Proc. Natl. Acad. Sci. U.S.A.* **2001**, *98*, 1404.

(11) Pandya, M. J.; Spooner, G. M.; Sunde, M.; Thorpe, J. R.; Rodger, A.; Woolfson, D. N. Sticky-end assembly of a designed peptide fiber provides insight into protein fibrillogenesis. *Biochemistry* **2000**, *39*, 8728−8734.

(12) Papapostolou, D.; Bromley, E. H. C.; Bano, C.; Woolfson, D. N. Electrostatic Control of Thickness and Stiffness in a Designed Protein Fiber. *J. Am. Chem. Soc.* **2008**, *130*, 5124−5130.
(13) Gunasekar, S. K.; Asnani, M.; Limbad, C.; Haghpanah, J. S.; Hom, W.; Barra, H.; Nanda, S.; Lu, M.; Montclare, J. K. N-Terminal Aliphatic Residues Dictate the Structure, Stability, Assembly, and Small Molecule Binding of the Coiled-Coil Region of Cartilage Oligomeric Matrix Protein. *Biochemistry* **2009**, *48*, 8559−8567.
(14) More, H. T.; Zhang, K. S.; Srivastiva, N.; Frezzo, J. A.; Montclare, J. K. Influence of Fluorination on Protein Engineered Coiled-coil Fibers. *Biomacromolecues* **2015**, *16*, 1210−1217.
(15) Hume, J.; Sun, J.; Jacquet, R.; Renfrew, P. D.; Martin, J. A.; Bonneau, R.; Gilchrist, M. L.; Montclare, J. K. Engineered Coiled-Coil Protein Microfibers. *Biomacromolecules* **2014**, *15*, 3503−3510.
(16) Gunasekar, S. K.; Anjia, L.; Matsui, H.; Montclare, J. K. Effects of Divalent Metals on Nanoscopic Fiber Formation and Small Molecule Recognition of Helical Proteins. *Adv. Funct. Mater.* **2012**, *22*, 2154−2159.
(17) Nivón, L. G.; Moretti, R.; Baker, D.; Pareto-Optimal, A. Refinement Method for Protein Design Scaffolds. *PLoS One* **2013**, *8*, No. e59004.
(18) Alford, R. F.; Leaver-Fay, A.; Jeliazkov, J. R.; O'Meara, M. J.; DiMaio, F. P.; Park, H.; Shapovalov, M. V.; Renfrew, P. D.; Mulligan, V. K.; Kappel, K.; Labonte, J. W.; Pacella, M. S.; Bonneau, R.; Bradley, P.; Dunbrack, R. L., Jr.; Das, R.; Baker, D.; Kuhlman, B.; Kortemme, T.; Gray, J. J. The Rosetta All-Atom Energy Function for Macromolecular Modeling and Design. *J. Chem. Theory Comput.* **2017**, *13*, 3031−3048.
(19) Kothiwale, S.; Mendenhall, J. L.; Meiler, J. BCL::Conf: small molecule conformational sampling using a knowledge based rotamer library. *J. Cheminf.* **2015**, *7*, 47.
(20) Park, H.; Zhou, G.; Baek, M.; Baker, D.; DiMaio, F. Force Field Optimization Guided by Small Molecule Crystal Lattice Data Enables Consistent Sub-Angstrom Protein−Ligand Docking. *J. Chem. Theory Comput.* **2021**, *17*, 2000−2010.
(21) Hill, L. K.; Britton, D.; Jihad, T.; Punia, K.; Xie, X.; Delgado-Fukushima, E.; Liu, C. F.; Mishkit, O.; Liu, C.; Hu, C.; Meleties, M.; Renfrew, P. D.; Bonneau, R.; Wadghiri, Y. Z.; Montclare, J. K. Engineered protein−iron oxide hybrid biomaterial for MRI-traceable drug encapsulation. *Mol. Syst. Des. Eng.* **2022**, *7*, 915−932.
(22) DeLano, W. L.The PyMOL Molecular Graphics System, 2002. http://pymol.org.
(23) Chennamsetty, N.; Voynov, V.; Kayser, V.; Helk, B.; Trout, B. L. Design of therapeutic proteins with enhanced stability. *Proc. Natl. Acad. Sci. U.S.A.* **2009**, *106*, 11937−11942.
(24) Cornell, W. D.; Cieplak, P.; Bayly, C. I.; Gould, I. R.; Merz, K. M.; Ferguson, D. M.; Spellmeyer, D. C.; Fox, T.; Caldwell, J. W.; Kollman, P. A. A Second Generation Force Field for the Simulation of Proteins, Nucleic Acids, and Organic Molecules. *J. Am. Chem. Soc.* **1995**, *117*, 5179−5197.
(25) Bas, D. C.; Rogers, D. M.; Jensen, J. H. Very fast prediction and rationalization of pKa values for protein−ligand complexes. *Proteins* **2008**, *73*, 765−783.
(26) Wang, P.; Bohr, W.; Otto, M.; Danzer, K. M.; Mizaikoff, B. Quantifying amyloid fibrils in protein mixtures via infrared attenuated-total-reflection spectroscopy. *Anal. Bioanal. Chem.* **2015**, *407*, 4015−4021.
(27) Hu, X.; Kaplan, D.; Cebe, P. Determining Beta-Sheet Crystallinity in Fibrous Proteins by Thermal Analysis and Infrared Spectroscopy. *Macromolecules* **2006**, *39*, 6161−6170.
(28) Jackson, M.; Mantsch, H. H. The use and misuse of FTIR spectroscopy in the determination of protein structure. *Crit. Rev. Biochem. Mol. Biol.* **1995**, *30*, 95−120.
(29) Schneider, C. A.; Rasband, W. S.; Eliceiri, K. W. NIH Image to ImageJ: 25 years of image analysis. *Nat. Methods* **2012**, *9*, 671−675.
(30) Meleties, M.; Britton, D.; Katyal, P.; Lin, B.; Martineau, R. L.; Gupta, M. K.; Montclare, J. K. High-Throughput Microrheology for the Assessment of Protein Gelation Kinetics. *Macromolecules* **2022**, *55*, 1239−1247.
(31) Meleties, M.; Katyal, P.; Lin, B.; Britton, D.; Montclare, J. K. Self-assembly of stimuli-responsive coiled-coil fibrous hydrogels. *Soft Matter* **2021**, *17*, 6470−6476.
(32) Hill, L. K.; Meleties, M.; Katyal, P.; Xie, X.; Xie, X.; Delgado-Fukushima, E.; Delgado-Fukushima, E.; Jihad, T.; Jihad, T.; Liu, C. F.; Liu, C. F.; O'Neill, S.; O'Neill, S.; Tu, R. S.; Tu, R. S.; Renfrew, P. D.; Renfrew, P. D.; Bonneau, R.; Bonneau, R.; Wadghiri, Y. Z.; Wadghiri, Y. Z.; Montclare, J. K. Thermoresponsive Protein-Engineered Coiled-coil Hydrogel for Sustained Small Molecule Release. *Biomacromolecues* **2019**, *20*, 3340−3351.
(33) Rai, D.; Singh, J. K.; Roy, N.; Panda, D. Curcumin inhibits FtsZ assembly: an attractive mechanism for its antibacterial activity. *Biochem. J.* **2008**, *410*, 147−155.
(34) Zsila, F.; Molnár, P.; Deli, J.; Lockwood, S. F. Circular dichroism and absorption spectroscopic data reveal binding of the natural cis-carotenoid bixin to human alpha1-acid glycoprotein. *Bioorg. Chem.* **2005**, *33*, 298−309.
(35) Yallapu, M. M.; Jaggi, M.; Chauhan, S. C. Curcumin nanoformulations: a future nanomedicine for cancer. *Drug Discovery Today* **2012**, *17*, 71−80.
(36) Nishad Fathima, N.; Saranya Devi, R.; Rekha, K. B.; Dhathathreyan, A. Collagen-curcumin interaction — A physico-chemical study. *J. Chem. Sci.* **2009**, *121*, 509−514.
(37) Fathima, N. N.; Dhathathreyan, A.; Ramasami, T. Directed 2-dimensional organisation of collagen: Role of cross-linking and denaturing agents. *J. Chem. Sci.* **2010**, *122*, 881−889.
(38) Arakawa, T. Acetonitrile as solvent for protein interaction analysis. *Int. J. Biol. Macromol.* **2018**, *114*, 728−732.
(39) Kwok, S. C.; Hodges, R. S. Stabilizing and destabilizing clusters in the hydrophobic core of long two-stranded alpha-helical coiled-coils. *J. Biol. Chem.* **2004**, *279*, 21576−21588.
(40) Lau, S. Y.; Taneja, A. K.; Hodges, R. S. Synthesis of a model protein of defined secondary and quaternary structure. Effect of chain length on the stabilization and formation of two-stranded alpha-helical coiled-coils. *J. Biol. Chem.* **1984**, *259*, 13253−13261.
(41) Shepherd, N. E.; Hoang, H. N.; Abbenante, G.; Fairlie, D. P. Left- and right-handed alpha-helical turns in homo- and hetero-chiral helical scaffolds. *J. Am. Chem. Soc.* **2009**, *131*, 15877−15886.

https://doi.org/10.1021/acs.biomac.2c01031
Biomacromolecules XXXX, XXX, XXX−XXX